ACS NANO

www.acsnano.org

ARTICLE

Intrinsically Stretchable and Printable Lithium-Ion Battery for Free-Form Configuration

Soo Yeong Hong, Sung Min Jee, Youngpyo Ko, Jinhan Cho, Keun Hyung Lee, Bongjun Yeom, Heesuk Kim, and Jeong Gon Son*

Cite This: *ACS Nano* 2022, 16, 2271−2281

Read Online

ACCESS | Metrics & More | Article Recommendations | Supporting Information

ABSTRACT: **For next-generation wearable and implantable devices, energy storage devices should be soft and mechanically deformable and easily printable on any substrate or active devices. Herein, we introduce a fully stretchable lithium-ion battery system for free-form configurations in which all components, including electrodes, current collectors, separators, and encapsulants, are intrinsically stretchable and printable. The stretchable electrode acquires intrinsic stretchability and improved interfacial adhesion with the active materials *via* a functionalized physically cross-linked organogel as a stretchable binder and separator. Intrinsically stretchable current collectors are fabricated in the form of nanocomposites consisting of a matrix with excellent barrier properties without swelling in organic electrolytes and nanostructure-controlled multimodal conductive fillers. Due to structural and materials freedoms, we successfully fabricate several types of stretchable lithium-ion battery that reliably operates under various stretch deformations with capacity and rate capability comparable with a nonstretchable battery over 2.5 mWh cm^{-2} at 0.5 C, even under high mass loading conditions over 10 mg cm^{-2}, including stacked configuration, direct integration on both sides of a stretch fabric, and application of various electrode materials and electrolytes. Especially, our stretchable battery printed on a stretch fabric also exhibits high performance and stretch/long-term stabilities in the air even with wearing and pulling.**

KEYWORDS: *stretchable lithium-ion battery, physically cross-linked organogels, stretchable current collector, all-component intrinsically stretchable battery, printing on stretch fabric*

Wearable and implantable electronics are of significant interest because of their wide range of potential applications, such as electronic skin, implantable health monitoring, and soft robotics for augmented reality.[1−5] Stretchability is an important property for the advancement to next-generation wearable electronics, which stably operate against mechanical deformations such as bending, twisting, and stretching. The power source is one component of wearable electronics, but the development of stretchable energy storage devices is lagging.[6] While other stretchable devices can simply achieve stretchability by miniaturization or thinning of active devices and leaning on the stretchability of the substrate, an energy storage device should be stretchable on its own because the amount of active materials are directly related to energy storage performance. However, only with hard inorganic active materials, it is very difficult to even operate the energy storage under mechanical deformation.[7−12]

The lithium-ion battery (LIB), the most commonly used rechargeable energy storage system due to its high energy density, long life, and low self-discharge rate, is composed of an anode and cathode, current collector, separator, electrolyte, and encapsulant.[13,14] To fabricate a stretchable full cell, all of these components must function reliably under mechanical deformation. Many structural approaches to specific components, especially electrodes, have been proposed for stretchable batteries, for example, wavy (buckled),[15,16] porous,[17,18] island−bridge (serpentine),[19] spring/textile,[20−23] and composite structures.[24−26] However, most structures acquire

Received: September 24, 2021
Accepted: January 14, 2022
Published: January 21, 2022

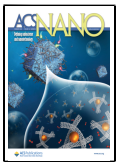

https://doi.org/10.1021/acsnano.1c08405
ACS Nano 2022, 16, 2271−2281

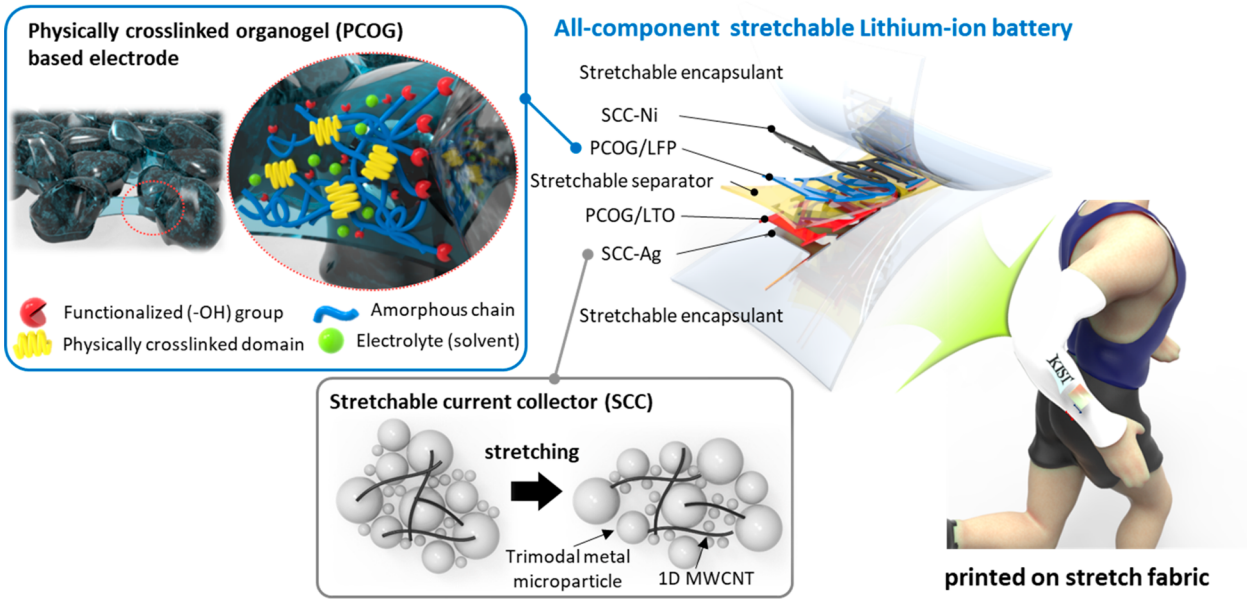

Figure 1. Schematic illustration of the assembled cell of the fully stretchable LIB based on PCOG/active materials, SCCs, stretchable PCOG separator, and stretchable encapsulant printed on stretch fabric. The PCOG and active materials composite electrode with the electrolyte contains physically cross-linked crystallite domains, swollen amorphous soft domains, and functionalized moieties to hold the active materials well, resulting in stable stretchability. The 1D carbon nanotube and multimodal metal microparticle nanocomposited SCCs also structurally maintain the multiple percolation paths even in the stretched state.

stretchability *via* prestraining or hybridization with a significant amount of elastomer that does not participate in energy storage, resulting in inevitably deteriorated energy storage performance in terms of volumetric/areal energy densities and rate capability. Also, most approaches have demonstrated only stretchability of a specific component rather than stretchability of the entire full-cell system. Although several stretchable full-cell batteries based on stretchable components recently have been reported,[27−29] realizing an ideal stretchable battery is still a long way off due to the lack of a stretchable current collector that stably maintains stretchability and conductivity even in contact with the electrolyte and a stretchable encapsulant that provides long-term stability in air. In addition, the greatest advantage of the stretchable device is best revealed in the free form. If all components have inherent stretchability and can be easily printed, then applications are infinite.

Herein, we report a fully stretchable LIB system based on intrinsically all-stretchable components, including electrodes, current collectors, separator, and encapsulant. Stretchable electrodes acquired intrinsic elasticity without adding an elastomer *via* physically cross-linked organogels (PCOGs) made from crystal growth control of polyvinylidene fluoride (PVDF), which is commonly used as a binder. Additionally, through its functionalization, adhesive properties were improved to suppress detaching from the active material under mechanical deformation, even with a small amount and even in solvent-soaked conditions. The PCOG was also used as a stretchable separator. The intrinsically stretchable and printable current collector (SCC) used a composite-based stretchable conductive adhesive technology previously reported by us[30] that incorporated multiscale metal microparticles and one-dimensional (1D) multiwalled carbon nanotubes (MWCNTs) as conductive fillers so that percolation could be well maintained even in the stretched state. Polyisobutylene (PIB), which has the best barrier properties among elastomers and does not swell in organic electrolytes, could be used as a matrix of the current collector and encapsulant to maintain stable stretchable battery performance for a long time. These approaches for stretchability and printability of each of all-components can provide the structural freedom of stretchable battery configurations along with material freedom of active materials and organic electrolytes. Our fully stretchable LIB demonstrated excellent energy storage performance over 130 mAh g^{-1} at 0.5 C without capacity degradation under 50% strain, showed stable electrochemical performance after 1000 times repetitive stretch/release cycles, and had superior long-term stability over 100 cycles under various deformations in an ambient air. Last, we first and successfully integrated a stretchable LIB full cell directly into a stretch fabric by double-sided sequential printing the electrodes and their current collectors each onto the stretch fabric used as a stretchable separator. The stretchable LIB integrated in stretch fabric of the arm-sleeve also showed high performance and mechanical stability under mechanical deformation such as wearing or stretching.

RESULTS AND DISCUSSION

Figure 1 presents schematic and detailed views of the multilayered structure of a fully stretchable LIB. The battery consists of a Ni-based cathodic SCC, PCOG/lithium iron phosphate (LFP) cathode, stretchable PCOG electrolyte/separator, PCOG/lithium titanate (LTO) anode, Ag-based anodic SCC, and PIB stretchable encapsulant. For the realization of intrinsically stretchable electrodes, we have noted interesting properties of PVDF, that is, it can form ion/organo gels with ionic liquids or carbonate electrolytes *via* crystallization from ketone solvents (inset image of Figure 1).[31,32] PVDF is widely used as a binder for electrodes because of high ionic conductivity and mechanical/electrochemical stabilities, but it is mainly used in the form of a poly(vinylidene fluoride-*co*-hexafluoropropylene) (PVDF-HFP) random co-

https://doi.org/10.1021/acsnano.1c08405
ACS Nano 2022, 16, 2271−2281

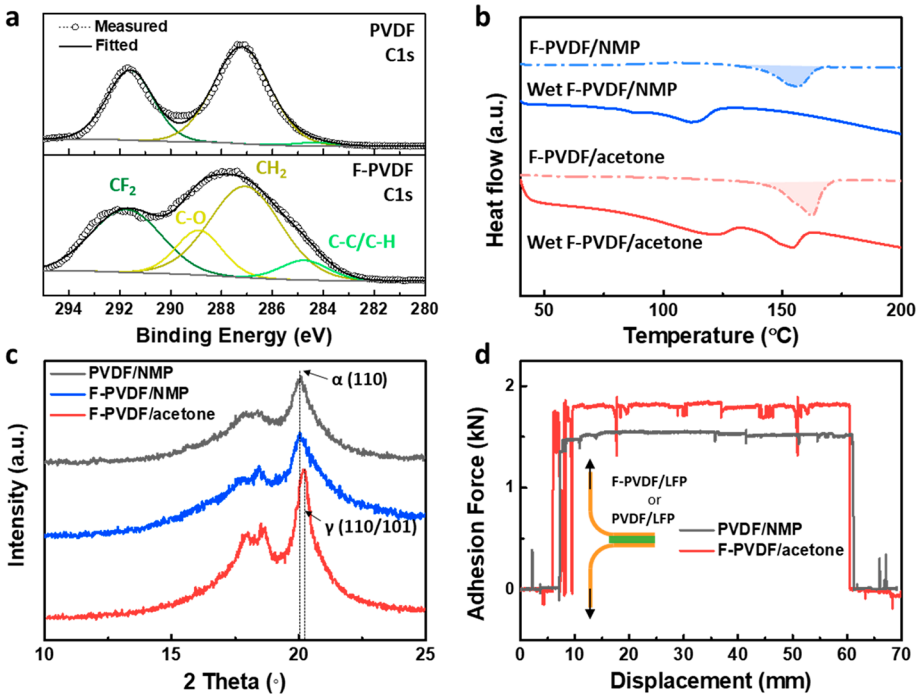

Figure 2. (a) X-ray photoelectron C 1s spectra of pristine PVDF and F-PVDF. (b) Differential scanning calorimetry analysis (10 °C min^{-1}) of first scanned profiles of dried F-PVDF films from acetone at room temperature (red dashed line), from NMP at 60 °C (blue dashed line), and F-PVDF films wetted with acetone (red solid line) and NMP (blue solid line). Fourier transform-infrared spectra of (c) PVDF powder (gray) and F-PVDF powder (red). (c) X-ray diffraction patterns of dried pristine PVDF film from NMP (gray), dried F-PVDF films from NMP (blue), and acetone (red), respectively. (d) Adhesion force measurements *via* peel test of the PVDF/LFP film and the PCOG/LFP film under dry state.

polymer, which does not readily form crystallites, because high crystallinity is not required for the binder. Rather, we implemented a stretchable organogel network using the high crystallinity of PVDF as rigid domains of an elastomer (mass) and swollen amorphous domains with high mobility from electrolyte/carbonate solvents as elastic springs of a mass–spring network.[31,32] In addition, for stretchability of the composite electrode, it is essential to prevent delamination at the interface between the active materials and the PCOG by strengthening the interfacial adhesion. We functionalized the PVDF with hydroxyl groups to increase adhesion with the active materials so that the microstructure of the electrodes could be maintained without delamination, even under mechanical deformation.

The hydroxyl group-functionalized PVDF (F-PVDF) polymer was produced according to the Fenton reaction.[33] Figure S1 presents X-ray photoelectron spectroscopy (XPS) survey spectra of pristine PVDF and F-PVDF and their chemical interpretation. Functionalization increased the intensity of the oxygen peak (O 1s) from 0% to 6.02% and reduced the intensity of the fluorine peak (F 1s) from 67.1% to 56.1%. A new intense C–O peak appeared at 288.9 eV (C 1s), while C–F peaks at 291.7 eV were less intense (Figure 2a).[34] The Fourier transform-infrared (FT-IR) spectrum of F-PVDF displayed a new absorption peak at 3350 cm^{-1}, which is characteristic of the hydroxyl group (Figure S2).[35] The partially hydroxylated F-PVDF promoted intimate interactions between the active materials.

Differential scanning calorimetric analysis of the F-PVDF films was performed in the dry state and in the wet state when immersed in liquid electrolyte (1 M $LiPF_6$ in ethylene carbonate/diethyl carbonate/dimethyl carbonate (EC/DEC/DMC), 1:1:1 vol %). Differences in crystallinity of the films after solvent evaporation and crystallite changes due to electrolyte wetting were investigated (Figure 2b). *N*-Methylpyrrolidone (NMP) is a good solvent and generally used in slurry preparations, while acetone is a marginal solvent. The melting temperature (T_m) of the dried F-PVDF films obtained from NMP and acetone was 156 and 162 °C, respectively. Acetone provided a more crystalline film, and gelation occurred during the evaporation process, forming a physically cross-linked (crystalline) structure. When wetted with the electrolyte (solid line in Figure 2b), the T_m of the crystallites formed from the NMP treatment shift to 112 °C, which indicated that the crystalline phase was completely swollen. However, two T_m peaks were observed for the crystallites formed from acetone treatment (red solid line in Figure 2b), with the low-temperature peak at 123 °C corresponding to partially swollen F-PVDF and the high-temperature peak at 154 °C to the unswollen cross-linked structure. This suggested that the rigid physically cross-linked structure could be maintained even if the film was soaked in electrolyte.

The crystalline phases of the PVDF film cast from NMP solution, and F-PVDF films cast from NMP and acetone solutions, were further characterized by FT-IR (Figure S2b). The PVDF film was predominantly α-phase, while the F-PVDF contained α- and γ-phase crystallites. X-ray diffraction analysis (Figures 2c and S3) revealed that the PVDF film contained relatively small (7.5 nm) α-phase crystallites, but the crystallites in the F-PVDF film were larger from acetone (16.9 nm) than from NMP (8.4 nm).[36,37] We believe that only the crystallites formed from acetone can provide physical cross-linking between polymer chains because the number of PVDF chains constituting the crystallite can be multiple only if the

https://doi.org/10.1021/acsnano.1c08405
ACS Nano 2022, 16, 2271–2281

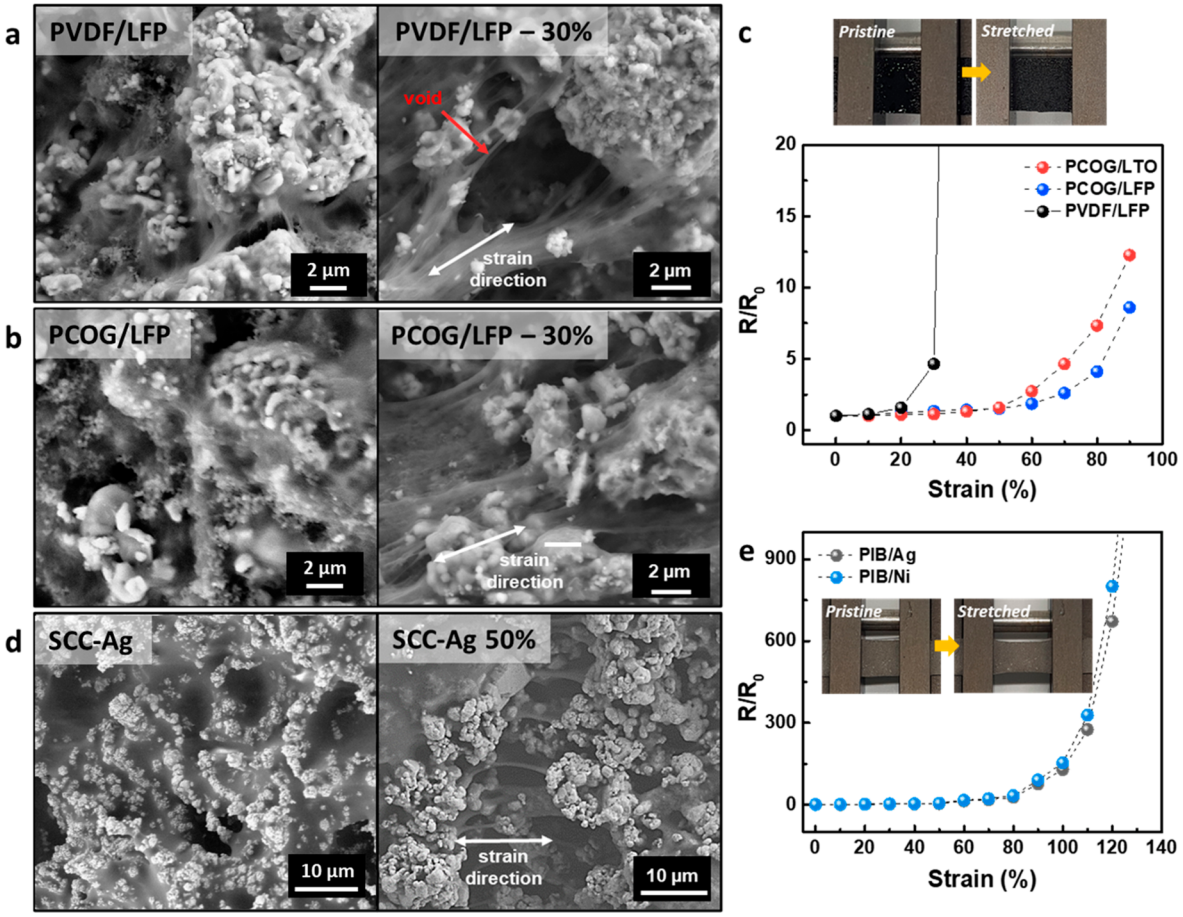

Figure 3. Scanning electron microscope images of (a) pristine PVDF/LFP and (b) PCOG/LFP cathodes, and (d) SCC-Ag under unstrained and 50% strained conditions. (c) Resistance as a function of strain of the PCOG/LTO anode (red), PCOG/LFP cathode (blue), and pristine PVDF/LFP cathode (black). (e) Resistance as a function of strain of SCC-Ag (gray) and SCC-Ni (blue).

size is at least close to the radius of gyration of PVDF (~12 nm, assuming a polydispersity index of ~2.25).[38] Further details can be found in the Supporting Information. Peel tests were performed to quantitatively measure the interfacial adhesions between the particles and the binders in the composite electrodes and the adhesions of the binders under wetted state with the electrolyte (Figures 2d and S4). F-PVDF/LFP and PVDF/LFP composite films (~150 μm) were attached between two sheets of 10 × 50 mm^2 polyimide (PI) films using a cyanoacrylate adhesive to prepare the specimens to be separated inside the films during the peel test. By measuring the cohesive strength of the composite films, the cohesive strength of the F-PVDF/LFP film was 1.2 times greater than that of the PVDF/LFP film (Figure 2d). This result means that the adhesion property between the F-PVDF and LFP particles constituting the composite electrode is greatly improved, because the hydroxyl group introduced by the functionalization process of F-PVDF increases the interfacial interaction with the LFP particles. Next, specimens were prepared by coating each binder solution on the PI film and attaching another PI film before drying (binder thickness: ~150 μm). The sandwiched films were immersed in 1 M $LiPF_6$ in EC/DEC/DMC electrolyte solution for 10 min prior to testing to examine the adhesion properties in the wet state. Adhesion force measurements under the wet state revealed that the adhesion strength of the F-PVDF film was much greater (~1.5-times) than that of pristine PVDF (Figure S4). Therefore, the F-PVDF-based PCOG stretchable composite electrode strengthens the interface between the active material and the binder, enabling it to maintain stretchability without fractures even with a small amount at the wet state in the electrolyte.

Stretchable anodes and cathodes were fabricated based on the composites of the PCOG and microparticle-type active materials and carbon black (weight ratio of 25:68:7), and stretchability was evaluated in the wet state. Scanning electron microscopy (SEM) images revealed that pristine PVDF/LFP particle composites contained numerous voids between the LFP particles and the PVDF and that delamination occurred at 30% strain due to poor adhesion (Figure 3a). In contrast, the PCOG uniformly covered LFP particles without voids and maintained the network without separation from particles even under 50% uniaxial strain (Figure 3b). Because the PCOG had physically cross-linked hard domains, partially swollen soft domains in the electrolyte, and functionalized groups for tight adhesion, the PCOG/LFP cathode remained stretchable under deformation even with low content of PCOG (inset of Figure 1). The PCOG/LTO composite anode also displayed a similar morphological stability under 50% strain (Figure S5a). The resistance of the PCOG/LTO anode, PCOG/LFP cathode, and pristine PVDF/LFP as a control group was measured at various strains to examine further the electrical properties under strain (Figure 3c). The electrical conductivities of the PCOG/LTO, PCOG/LFP, and PVDF/LFP were 3.1, 1.63,

https://doi.org/10.1021/acsnano.1c08405
ACS Nano 2022, 16, 2271−2281

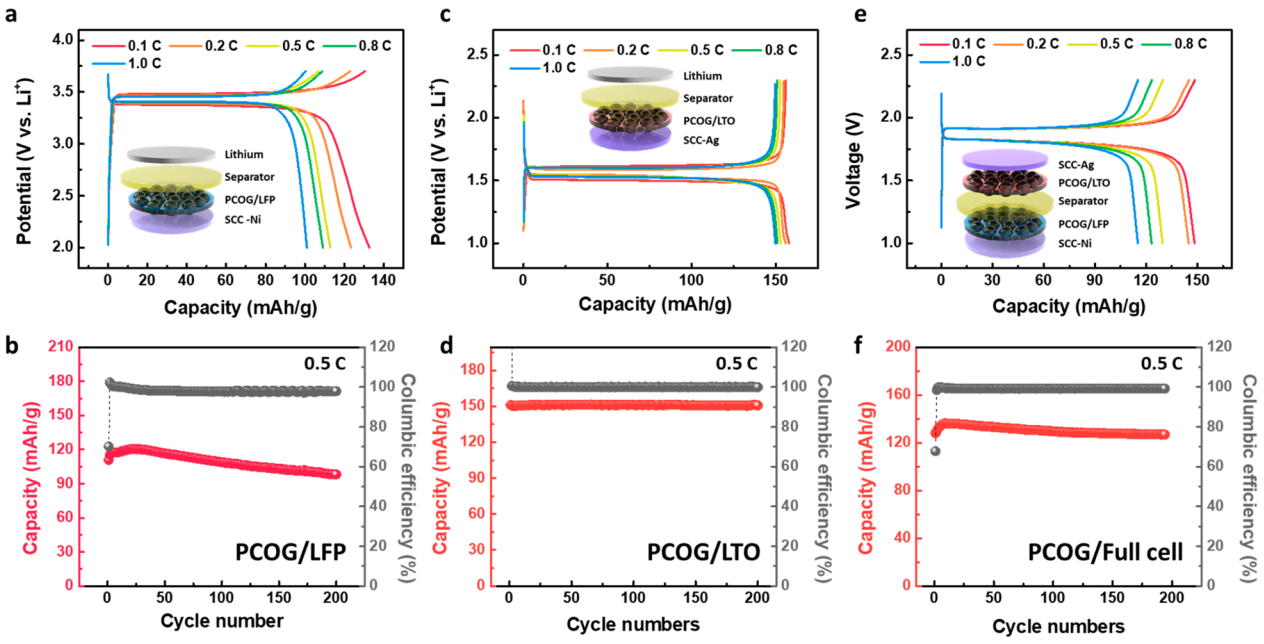

Figure 4. Schematic illustrations and electrochemical performances of PCOG-based composites. (a, b) Cathode, (c, d) anode, and (e, f) full cell. Representative charge/discharge curves of (a) PCOG/LFP between 2 and 3.7 V, (c) PCOG/LTO between 1 and 2.3 V, and (e) PCOG/LFP and PCOG/LTO full cell between 1 and 2.3 V. Cycling performances and Coulombic efficiencies of (b) PCOG/LFP and (d) PCOG/LTO half cells and (f) PCOG/LFP and PCOG/LTO full cells at 0.5 C.

and 1.58 S cm^{-1}, respectively. The resistances of the PCOG-based cathode and anode were almost unchanged until 50% strain, started to increase at 60%, and were 8-fold higher at 90% strain, while the pristine PVDF/LFP electrodes broke at 40% strain. We also tested the durability of the electrical properties of the stretchable cathode and anode. Highly stable electrode material connections with little change in resistance were observed even after 5000 stretching/releasing cycles at strains up to 50% (Figure S6a). Our approach that imparts stretchability and interfacial adhesion to typical binder materials used in conventional LIBs could become a much more universally applied and influential technology for a stretchable battery, as current materials and processes can be used as is.

Next, when the intrinsically SCC can be introduced using a printing process, a print-type stretchable battery can be introduced on any substrate or next to other stretchable active devices such as glucose sensors, with a variety of structural freedoms, from stacked to 3D interdigitated configurations. While the intrinsic and printable SCC is rarely used in stretchable batteries yet (Table S1), we fabricated it using our nanocomposite-based architecture-controlled technology.[30] Various multiscale metal microparticles (Ag particles for the anode, Ni particles for the cathode; 74.8 wt %) can be widely selected as the conductive fillers, and 1D MWCNTs (0.2 wt %) were used as an auxiliary filler to induce elongated phase separation and a networked structure to facilitate percolation formation and maintenance in the stretched state. The SCC matrix should stably maintain stretchability and percolation paths without swelling or other structural changes during the electrode coating process and immersing in the electrolyte. Also, if the electrolyte swells the current collector unnecessarily, a large amount of electrolytes is required and the electrolyte drought occurs quickly. To identify these materials, we measured the swelling ratios of typical elastomer films including PIB and PDMS under the saturated vapors of liquid electrolytes (Figure S7). The thickness change (swelling ratio, $S = t/t_0$) of PIB film was 1 (almost no change), whereas PDMS, which is the most commonly used elastomer in stretchable batteries, swelled significantly to 2.25. The PIB solution also has orthogonality with the electrode coating solution, allowing additive printing in any order. In addition, the PIB is a material commonly used as an adhesive in industry and has the advantage of preventing delamination between the electrodes and the SCCs, so the PIB was adopted as the matrix of the SCC (24.9 wt %).

The 200 μm-thick SCC-Ag and SCC-Ni electrodes were prepared by a doctor-blade method and dried at 60 °C for 2 h. Figures 3d and S5b present SEM images of the PIB/Ag and PIB/Ni SCCs under unstrained and 50% strain conditions. The Ag and Ni particles were uniformly distributed in the PIB in the initial state, and the conductive particles, at 50% strain, maintained a dense conductive network within elongated bridges due to the elastic properties of PIB. The electrical conductivities of the SCC-Ag and SCC-Ni electrodes were 3912 and 2105 S cm^{-1}, respectively, and the resistance changes as a function of uniaxial strain are shown in Figure 3e. The SCC-Ni and SCC-Ag electrodes exhibited slight increases from the unstrained to the 50% strain condition, respectively, and stable deformation up to 130% strain. Additionally, the resistance changes over 5000 cycles at 50% strain were 1.22 and 1.24, respectively, indicating excellent electrical stability during repeated stretching cycles (Figure S6b). The MWCNTs made the effective interparticle interactions between the Ag conductive particles more attractive, causing excellent electrical stability and thereby rendering the percolating network relatively stable (Figure S8).[30]

The effect of the PCOG/active materials and SCCs on the electrochemical performance of LIBs was investigated. The PCOG/LTO anode and PCOG/LFP cathode were prepared by slurry-coating the active materials onto the SCC-Ag and SCC-Ni surfaces. Galvanostatic testing was conducted in half-

https://doi.org/10.1021/acsnano.1c08405
ACS Nano 2022, 16, 2271−2281

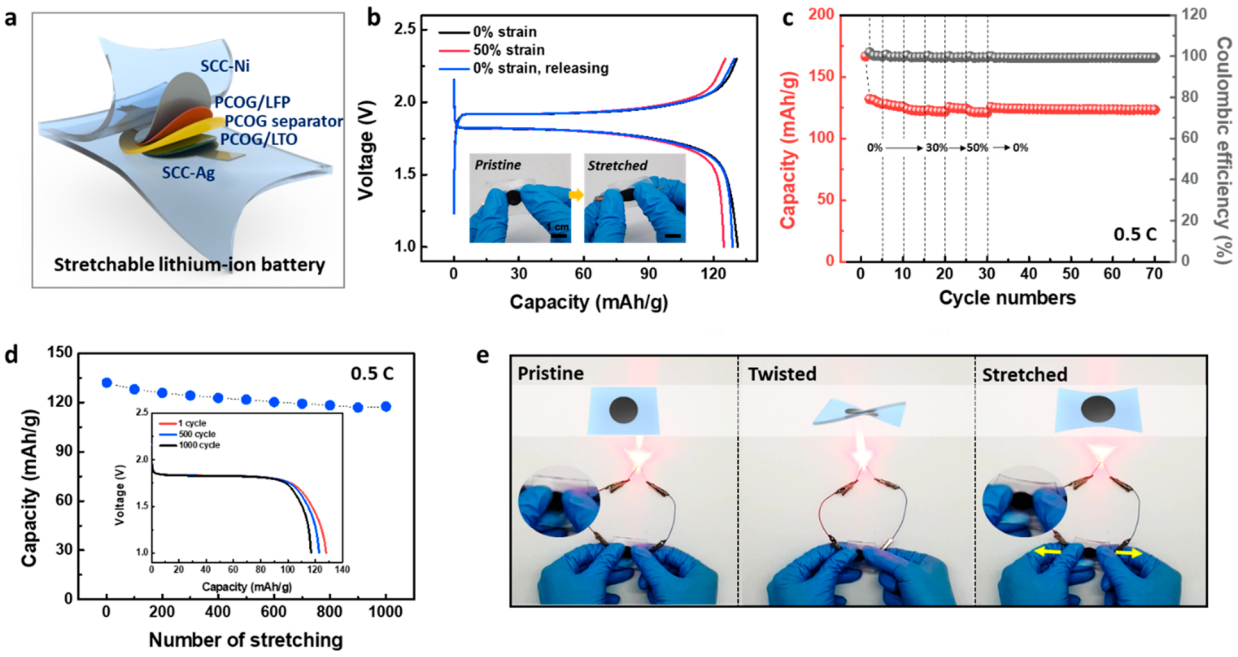

Figure 5. (a) Schematic illustration of the fabricated stretchable battery. (b) Charge/discharge curves of the stretchable battery in the unstretched (black), 50% stretched (red), and released (blue) states at 0.5 C. (c) Discharge capacity of the stretchable battery ranging from 0% to 50% strain for five cycles at 10% intervals to 70 cycles at 0.5 C. (d) Capacity change under repetitive stretching/releasing between 0% and 50% strain. (e) Photographs of the stretchable battery in various deformation states turning on a light-emitting diode bulb.

cell configurations using a standard 2032-type coin cell with lithium metal as counter electrodes, the PCOG as separator, and 1 M $LiPF_6$ in EC/DEC/DMC (1:1:1 vol %) as electrolyte (Figure 4a,c). The PCOG wetted with electrolyte also displayed good stretchability and transparency due to physical cross-linking, so it can be applied as a stretchable separator, as shown in our previous study[24] and Figure S9. The ionic conductivities of the PCOG and PP separators were 0.986 and 0.518 mS cm^{-1}, respectively, which provided a slightly higher mobility to ions (Figure S10), and electrolyte uptake of the dried PCOG separator was over 250% (Figure S11). The galvanostatic electrochemical and rate performances of the PCOG/LFP cathode were 135, 121, 112, 102, and 99 mAh g^{-1} of specific capacities at rates of 0.1, 0.2, 0.5, 0.8, 1, and 3 C, respectively (Figures 4a and S12a). In addition, the PCOG/LTO anode displayed corresponding values of 158, 156, 153, 151, and 150 mAh g^{-1} at rates of 0.1, 0.2, 0.5, 0.8, 1, and 3 C, respectively (Figures 4c and S12b). Figure 4b,d presents retention test results for the PCOG/LFP cathode and PCOG/LTO anode conducted at the rate of 0.5 C. The specific capacities of the electrodes were 85% and 99%, respectively, after 200 cycles. The Coulombic efficiencies at 0.5 C were close to 100%. We also used mesocarbon microbeads (MCMB) graphite powder with this PCOG to fabricate a stretchable anode and achieved a high performance of 230 mAh g^{-1} at 0.5 C (Figure S13a). This result confirmed the great cycling performance, high reversibility, and material versatility of the intrinsically stretchable cathode and anode.

The electrochemical performance of the full-cell assembly of the PCOG/LFP cathode and PCOG/LTO anode with the SCCs in a coin-cell configuration without strain was measured using a stretchable PCOG as a separator (inset of Figure 4e). Figure 4e presents the galvanostatic charge/discharge curves over the range of 1−2.3 V for the stretchable full cell in the presence of 1 M $LiPF_6$ electrolyte. It was conducted based on the active material of the anode. The rate capability of the full cell (Figure 4f) was evaluated at 0.2 and 1 C; specific capacities of 149 and 112 mAh g^{-1}, respectively, were obtained. Figure S12c presents the cycling performance of the stretchable PCOG full cell at a rate of 0.5 C; the full cell exhibited a highly stable discharge capacity of 128 mAh g^{-1} at 0.5 C, which resulted in 99% capacity retention after 200 cycles. In addition, the full cell of PCOG/LFP and PCOG/MCMB was also fabricated, exhibiting capacity of 142 mAh g^{-1} at 0.5 C with an operating voltage of 3.3 V (Figure S13b), confirming successful operation. Using an ionic liquid instead of carbonate solvents in the same cell, the storage performance of 128 mAh g^{-1} at 0.5 C was demonstrated, confirming that our cell can use a variety of electrode and electrolyte materials and can be nonflammable (Figure S14).

An all-stretchable-component LIB was assembled by sequentially stacking the SCC-Ni, PCOG/LFP cathode, stretchable PCOG separator, PCOG/LTO anode, SCC-Ag, and PIB encapsulation substrate (Figure 5a). Each component in the stretchable LIB was fabricated by a solution doctor-blading process. This all-printable solution process provides free-form form factors for stretchable batteries, greatly increasing their applicability. The thicknesses of the anode electrode, PCOG separator, and cathode electrode were 100, 20, and 100 μm, respectively, and the total thickness of the stretchable LIB was <1 mm, including the encapsulation layers. The PIB was also used as an encapsulating material because it exhibited the highest barrier properties among elastomers and does not swell in organic electrolytes (Figure S7). The electrochemical performance of the fully stretchable full cell was measured at various current rates over the range of 1−2.3 V (Figure S15). The discharge capacities were 144, 137, 128, 121, and 112 mAh g^{-1} at 0.1, 0.2, 0.5, 0.8, and 1 C, respectively, indicating good rate capability even in the stretchable cell configuration. The areal and volumetric

https://doi.org/10.1021/acsnano.1c08405
ACS Nano 2022, 16, 2271−2281

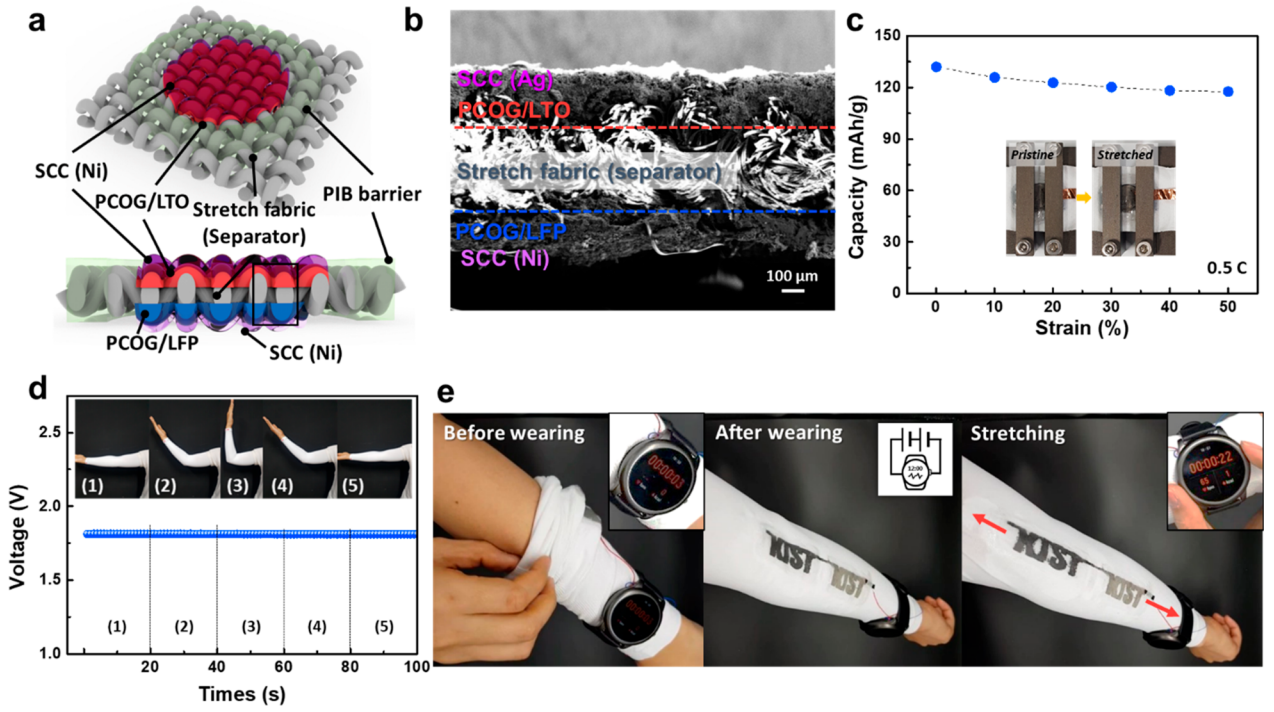

Figure 6. (a) Schematic illustration of the stretchable battery printed on stretch fabric consisting of printable stretchable electrodes, SCCs, encapsulant, and fabric as a stretchable separator. (b) Scanning electron microscope cross-sectional image of the stretchable battery printed on the stretch fabric. (c) Capacity change as a function of strain. (d) Change in the voltage and current of stretchable battery printed on the stretch arm sleeve under various angled deformations at the elbow. (e) Photographic images of a continuously operated smart watch connected with the stretchable LIB printed our institute name on the stretch fabric before and after wearing and stretching.

capacities were 1.5 mAh cm^{-2} and 3.75 mAh cm^{-3} at 0.5 C (the total thickness of the anode, cathode, and separator was ~0.4 mm). The areal and volumetric energy densities were 2.3 mWh cm^{-2} and 57.5 mWh cm^{-3}, respectively. We also investigated the long-term stability of the organic electrolyte-based stretchable LIB full cell in ambient air; this is not reported in most stretchable battery studies. The capacity retention of our fully stretchable LIB at the current rate of 0.5 C was a very high ~92% after 110 cycles in ambient air, not in a glovebox.

The mechanical stability of the fully stretchable LIB was evaluated under various conditions in air. Exhibiting a discharge capacity of 131 mAh g^{-1} at 0.5 C before tensioning, it maintained high values of 124 and 128 mAh g^{-1} at 50% strain and upon returning to 0% strain, respectively (Figure 5b). Cycling tests at 0.5 C under various strains ranging from 0% to 50% at 10% intervals were performed for five cycles each (Figure 5c). The fully stretchable LIB exhibited little change in charge/discharge characteristics even under the various strain conditions (capacity retention of 92% at 50% strain) and also showed long-term stability over 70 cycles even under the stretching test. After 1000 cycles of repetitive stretching/releasing at 50% strain, the fully stretchable LIB also retained over 89% of its discharge capacity at 0.5 C (Figure 5d). In addition, the stretchable full battery with PCOG/MCMB and PCOG/LFP electrodes stably maintained the capacity of 132 mAh g^{-1} at 0.5 C (93% of retention compared to flat state) with an operating voltage of 3.2−3.35 V even in a bending test with a 2 mm radius of curvature (Figure S16). These excellent mechanical stabilities originated from the deformability of the PCOG electrodes and SCCs (Figure 3). No delamination or voids were observed between the electrode and the SCC after 100 cycles of repeated stretching/releasing at 50%, as shown in SEM images in Figure S17. Table S1 compares the capacity, energy density, strain stability, repetitive strain stability, long-term stability, and stretch strategies of each component, including the current collector and encapsulant, with previously reported nonaqueous stretchable batteries. Our stretchable LIB has demonstrated superior areal capacity and energy density with excellent rate capability at a high mass loading compared to other stretchable batteries, exhibited various types of stretchable batteries through the versatility of materials and printability of all components, and confirmed mechanical stabilities under various deformations resulting from the intrinsic stretchability of all components.[12−14,16−22,25,39] Figure 5e shows that the fully stretchable LIB could operate a light-emitting diode under various deformations, such as twisting and stretching, which indicates that it could supply power even under external strain (Movie S1).

Our fully stretchable LIB can be manufactured using a printing process, greatly increasing structural freedom and allowing integration even with a stretchy fabric. A fabric-based stretchable LIB could be operated as a mobile display or smart watch for health monitoring systems (Figure 1). Figure 6a illustrates the case where the stretch fabric itself acted as a stretchable separator and had stretchable electrodes and SCCs coated on both sides by stencil printing. As far as we know, using stretch fabric as a separator, and fabricating printed cells in a laminated form on stretch fabric, has not been attempted before. It was then encapsulated with a PIB film/resin, and 1 M $LiPF_6$ electrolyte was injected into the cell. Cross-sectional SEM images and corresponding elemental mapping confirmed conformal coating of the high mass loading (11.7 mg cm^{-2})

https://doi.org/10.1021/acsnano.1c08405
ACS Nano 2022, 16, 2271−2281

PCOG/LFP cathode and PCOG/LTO anode on the 500 μm-thick stretch fabric and well-defined areas (Figures 6b and S18). We confirmed through impedance measurements (Figure S10) and electrolyte uptake (>300%, Figure S11) that the stretch fabric could function effectively as a stretchable support and battery separator. Electrochemical performance and retention testing of the fabric-based stretchable LIB were measured at various current rates in ambient air (Figure S19). The capacities of the stretchable LIB on the stretch fabric were 132 and 117 mAh g^{-1} at 0% and 50% strain, respectively, with 88% capacity retention at 50% strain (Figure 6c), and the areal capacity and energy density of 1.54 mAh cm^{-2} and 2.8 mWh cm^{-2}, respectively, are the highest in organic-based intrinsic stretchable batteries. In addition, decent long-term stability of the stretch fabric-based stretchable LIB was confirmed with a capacity retention of 90% at 0.5 C after 80 cycles in air (Figure S19b). The high performance, little change in capacity, and long-term stability in air confirmed that all of the components and printed SCC lead tabs were also tightly attached to the stretch fabric and operated stably under mechanical deformations. Figures 6d and S20 present the discharge voltages for different degrees of elbow bending of a stretchable LIB fabricated on stretch arm sleeve fabric with dimensions of 5.2 × 2 cm^2 and worn on the elbow. The voltage was almost unchanged despite the large deformation through varying the elbow bending angle. Practically, two stretchable LIBs printed on a stretched arm sleeve were connected in series and successfully operated a smart watch (operating at 3.7 V, Figure S21) under various deformations, such as putting on, taking off, and stretching the arm sleeve and moving the elbow (Figure 6e and Movie S2). These results clearly demonstrate the excellent mechanical stability of our stretchable LIB based on PCOGs, SCCs, and stretchable separator and encapsulations and indicate their great potential for applications in wearable and skin-attachable electronics as integrated energy storage devices.

CONCLUSIONS

We developed an all-component intrinsically stretchable and printable LIB system, including the electrodes, current collectors, separator, and encapsulant. Physically cross-linked organogels with functionalization introduced into the electrodes and the separator simultaneously facilitated access to the electrolyte and ensured an elastic stability and higher adhesion property within a small volume fraction. An approach that imparts stretchability and interfacial adhesion to conventional binder materials with high ionic conductivity used in conventional LIBs could become a much more universally applied and influential key technology. By introducing a stretchable current collector as a printing method based on a composite ink, the freedom of battery structures, such as direct printing on any substrate or next to other stretchable active devices, or 3D interdigitate construction as well as stacked structures, and the freedom of material to select metal particles easily and widely according to the operating voltage, could be obtained. With these intrinsically stretchable and printable components, the stretchable LIB with superior areal capacity and energy density even comparable to nonstretchable batteries with excellent rate capability at a high mass loading could be fabricated. Also, various types of stretchable batteries could be fabricated through a variety of materials and printability of all components, and mechanical stability under various deformations, including excellent retention rates under strain and after repeated stretching/releasing cycles and long-term stability under deformed state, could be obtained. Finally, this stretchable battery system was directly printed on stretch fabric with a stacked configuration. The stretchable battery integrated into the stretch fabric maintains a high specific capacity and areal energy density even when using the stretch fabric as a stretchable separator, exhibiting superior mechanical stability to operate the wearable watch during pulling on, taking off, and stretching. As our stretchable and printable battery has a comparable energy storage performance to nonstretchable batteries, along with a wide variety of material applicability and flexibility of structural form factors, it can be positioned as a promising platform for free-form stretchable batteries for the development of next-generation wearable or implantable electronic devices.

METHODS

Materials. PDMS (Sylgard 184, Dow corning), polyurethane (PU, C85A, BASF), styrene-ethylene-butylene-styrene (SEBS, G1657M, KRATON) dissolved in solvent with *n*-hexane (Sigma-Aldrich), dimethylforamide (DMF, Sigma-Aldrich), chloroform (Sigma-Aldrich), respectively, were used for the swelling test of the encapsulant film. Polyisobutylene (PIB, average M_w = 1,000,000, Sigma-Aldrich) was dissolved in toluene (Sigma-Aldrich) to make the encapsulant film. Active materials of the $Li_4Ti_5O_{12}$ (LTO, MTI Corporation), $LiFePO_4$ (LFP, EQ-Lib-LFPO-S21, MTI Corporation), and mesocarbon microbeads (MCMB, MTI Corporation) were used. Polyvinylidene fluoride (PVDF, weight-averaged M_w = 534,000, powder, Sigma-Aldrich), poly(vinylidene fluoride-*co*-hexafluoropropylene) (PVDF-HFP, average M_w = 400,000, pellets, Sigma-Aldrich), and acetone (Sigma-Aldrich) were used for the PCOG film. To make the commercial battery electrode, *N*-methyl-2-pyrrolidone (NMP, Sigma-aldrich) solvent was used. For the stretchable current collector, 150 nm, 2−3.5 μm, and 5−8 μm Ag particles (Sigma-Aldrich), 100 nm, 1 μm, and 50 μm Ni particles (Sigma-Aldrich), and a multiwalled carbon nanotube (MWCNT, length = 20−100 μm, average diameter = ∼20 nm, purity >95 wt % CNT Co., Ltd.) were purchased.

Fabrication of Stretchable PCOG/Active Material Electrodes. The hydroxyl group-containing functionalized PVDF (F-PVDF) was produced by the Fenton reaction.[33] The neat PVDF powder (5 g), 0.695 g of $FeSO_4{\cdot}7H_2O$ (Sigma-Aldrich), and 25 mL of hydrogen peroxide with 35 wt % were mixed in ethanol (25 mL) by stirring for 2 h at 50 °C. The resultant product was filtered and washed thoroughly with 1 M H_2SO_4 (DAEJUNG), and the iron salt adsorbed on the polymer was removed. The F-PVDF was then dried in a vacuum oven overnight. The obtained F-PVDF powder (110 mg) was dissolved in acetone (3 mL) to make a viscous liquid. Active materials (LFP, LTO, MCMB) and super P (carbon black) were then added in a weight ratio of 25:68:6.8 F-PVDF:active material:super P. The slurries were mixed using a Thinky mixer ARV-310 (Thinky Corporation) at 2000 rpm for 7 min. The fabricated slurries were doctor bladed onto SCCs (300 μm of thickness and 5 mm s^{-1} of speed) and then dried for 10 min at room temperature and vacuum over overnight. In order to compare the performance with F-PVDF, pristine PVDF was dissolved in NMP. The pristine PVDF-based paste with NMP was doctor bladed and dried at 130 °C.

Fabrication of SCCs. 1 g of the PIB was dissolved in chloroform (7 mL) for 3 h at 60 °C. 3 g of Ag particle (mixed with a size of 150 nm, 2−3.5 μm, and 5−8 μm) and 10 mg of MWCNTs were mixed, and the PIB solution was added to the powder mixture, followed by mixing using a Thinky mixer at 2000 rpm for 7 min. The solution was doctor bladed onto a glass substrate. The film was dried at 60 °C for 2 h. Likewise, Ni particles (mixed with a size of 100 nm, 1 μm, and 50 μm), MWCNTs, and PIB were mixed to make a SCC for the cathode. The thickness of the fabricated SCC-Ag, SCC-Ni was 300 μm.

Preparation of Stretchable PCOG Separator. The PVDF-HFP pellet was dissolved in acetone at a weight ratio of 1:7 PVDF-HFP:acetone at 50 °C for 1 h. The PVDF-HFP solution was doctor

https://doi.org/10.1021/acsnano.1c08405
ACS Nano 2022, 16, 2271−2281

bladed onto the glass substrate. The film was then immersed in a water bath for 3 h and dried under vacuum at 70 °C for 6 h. After that, the dense surface of film was removed using an oxygen RIE process (Femtoscience Inc. VITA, O_2 20 sccm, 20 mTorr, 100 W, 25 min). Before the battery was assembled, the PCOG separator was fully soaked with the electrolyte (1 M $LiPF_6$ in EC/DEC/DMC (1:1:1 vol %)).

Fabrication of Stretchable LIB. The screen-printed anode and cathode on SCCs (mass ratio of LFP:LTO of 1:1.3 and LFP:MCMB of 2.3:1) were attached to the PIB encapsulant films and immersed in the electrolyte (1 M $LiPF_6$ in EC/DEC/DMC (1:1:1 vol %) or LiTFSI with EMIMTFSI (1:1 of weight ratio) for nonflammability) over 1 h at room temperature. The prepared PCOG separator was placed on one electrode. The PIB resin (5 wt % PIB in toluene) was applied like an adhesive around the electrodes of the PIB films, and then two electrode films were laminated. After attaching the PIB encapsulation film, the electrolyte was injected through a syringe.

Stretchable LIB on Stretch Fabric. To print the stretchable battery to stretch fabric, a paper mask with our institute name was prepared using a cutting machine (Silhouette, Lindon, UT, USA). The fabricated mask attached to the stretch fabric and the slurries of PCOG/active materials were doctor bladed onto the stretch fabric and dried (mass loading of 11.7 mg cm^{-2}). Then the SCC slurry was also screen-printed onto the coated PCOG/active materials and dried. Next, it was flipped over, and the opposite electrode and the SCC were coated with the mask through the same process. The PIB resin was applied onto the stretch fabric using a brush to prevent electrolyte leakage. Finally, after attaching the PIB encapsulation film, the electrolyte was injected through a syringe.

Characterization. Surface morphology and cross-section of the fabricated stretchable electrodes and SCCs were observed using scanning electron microscopy (SEM, Sigma 300, ZEISS). The chemical structure of the PVDF and F-PVDF were investigated by Fourier transform-infrared (FT-IR) spectroscopy (Nicolet 380; Thermo Fisher Scientific Inc.) and X-ray photoelectron spectroscopy (XPS, K-Alpha+; Thermo Fisher Scientific) employing an Al Kα source (1486.6 eV). The energy step and X-ray spot size were 0.1 eV and 500 nm, respectively. The argon-ion beam was exposed for 1 s to remove surface contamination of the PVDF. A curve fitting program by Avantage software was used to fit XPS peaks with one or more Gaussian-Lorentz functions. The melting behaviors of the wetted F-PVDF and PVDF were analyzed using differential scanning calorimetry (DSC, DSC7, PerkinElmer) after the dried films were immersed in electrolyte for 30 min. The sample was measured at the first heating scan at 10 °C/min from 30 to 300 °C. The X-ray diffractometer (XRD, D/max2500/PC, Rigaku) was operated at 60 kV and 30 mA with Cu goniometer radius 185 mm. A universal testing machine (UTM, 5567, Instron) was used to perform the adhesion properties of the PCOGs immersed in electrolyte while soaking for 30 min for the wet-state and cohesion properties in a dry-state by attaching the film with an instant adhesive (cyanoacrylate, Loctite 406, Henkel Ltd.). The electrochemical properties were obtained using galvanostatic measurements with a battery tester (WBCS3000, WonAtech).

ASSOCIATED CONTENT

Supporting Information

The Supporting Information is available free of charge at https://pubs.acs.org/doi/10.1021/acsnano.1c08405.

XPS, FT-IR, XRD spectra of pristine PVDF, F-PVDF, PVDF/NMP, F-PVDF/NMP, and F-PVDF/acetone films, peel testing while immersed in electrolyte, SEM images of stretchable anode and current collectors at unstained and 50% strained states, resistance changes of the electrodes and current collectors under repetitive stretching/releasing, swelling ratio measurement of PIB, SEBS, PDMS, and PU, photographs of the stretchable gel electrolyte, Nyquist plots and electrolyte uptake of the separators, rate performance and Coulombic efficiencies of half/full cells, charge/discharge curves with mesocarbon microbeads anode, electrochemical performance of full cell with ionic liquid electrolyte, rate performance, cycling performance and Coulombic efficiency of fully stretchable LIB full cell with stretchable encapsulation and printed on stretch fabric, stretchable LIB full cells under the various bending conditions, SEM observation of interfaces between the stretchable electrodes and stretchable current collectors, EDS spectrum of the printed stretchable battery on stretch fabric, comparison table of materials and performances in previous research of stretchable full cell battery (PDF)

Movie S1: The stretchable battery in various deformation states turning on a light-emitting diode bulb (MP4)

Movie S2: Continuously operated smart watch connected with the stretchable LIB printed our institute name on the stretch fabric before and after wearing and stretching (MP4)

AUTHOR INFORMATION

Corresponding Author

Jeong Gon Son − *Soft Hybrid Materials Research Center, Korea Institute of Science and Technology, Seoul 02792, Republic of Korea; KU-KIST Graduate School of Converging Science and Technology, Korea University, Seoul 02841, Republic of Korea;* orcid.org/0000-0003-3473-446X; Email: jgson@kist.re.kr

Authors

Soo Yeong Hong − *Soft Hybrid Materials Research Center, Korea Institute of Science and Technology, Seoul 02792, Republic of Korea*

Sung Min Jee − *Soft Hybrid Materials Research Center, Korea Institute of Science and Technology, Seoul 02792, Republic of Korea*

Youngpyo Ko − *Soft Hybrid Materials Research Center, Korea Institute of Science and Technology, Seoul 02792, Republic of Korea; KU-KIST Graduate School of Converging Science and Technology, Korea University, Seoul 02841, Republic of Korea*

Jinhan Cho − *Department of Chemical and Biological Engineering and KU-KIST Graduate School of Converging Science and Technology, Korea University, Seoul 02841, Republic of Korea;* orcid.org/0000-0002-7097-5968

Keun Hyung Lee − *Department of Chemistry and Chemical Engineering, Inha University, Incheon 22212, Republic of Korea;* orcid.org/0000-0003-4066-9991

Bongjun Yeom − *Department of Chemical Engineering, Hanyang University, Seoul 04763, Republic of Korea;* orcid.org/0000-0001-8914-0947

Heesuk Kim − *Soft Hybrid Materials Research Center, Korea Institute of Science and Technology, Seoul 02792, Republic of Korea;* orcid.org/0000-0002-0898-7781

Complete contact information is available at: https://pubs.acs.org/10.1021/acsnano.1c08405

Notes

The authors declare no competing financial interest.

https://doi.org/10.1021/acsnano.1c08405
ACS Nano 2022, 16, 2271−2281

ACKNOWLEDGMENTS

We gratefully acknowledge financial support from the Korea Institute of Science and Technology (KIST) and KU-KIST Institutional Program (project No. 2E31811 and 2V06630) and the National Research Foundation of Korea (NRF) grant funded by the Korea government (MEST) (2019R1A2C2005657, 2021R1C1C2007738, and 2022R1A2B5B02001597). In addition, the Creative Materials Discovery Program also supported this work through the NRF grant funded by the Ministry of Science and ICT (2020M3D1A1110499, 2020M3D1A2101799, and 2020M3D1A2101800).

REFERENCES

(1) Hong, S. Y.; Kim, M. S.; Park, H.; Jin, S. W.; Jeong, Y. R.; Kim, J. W.; Lee, Y. H.; Sun, L.; Zi, G.; Ha, J. S. High-Sensitivity, Skin-Attachable, and Stretchable Array of Thermo-Responsive Suspended Gate Field-Effect Transistors with Thermochromic Display. *Adv. Funct. Mater.* **2019**, *29* (6), 1807679.

(2) Yamamoto, Y.; Yamamoto, D.; Takada, M.; Naito, H.; Arie, T.; Akita, S.; Takei, K. Efficient Skin Temperature Sensor and Stable Gel-Less Sticky ECG Sensor for a Wearable Flexible Healthcare Patch. *Adv. Healthc. Mater.* **2017**, *6* (17), 1700495.

(3) Son, D.; Kang, J.; Vardoulis, O.; Kim, Y.; Matsuhisa, N.; Oh, J. Y.; To, J. W. F.; Mun, J.; Katsumata, T.; Liu, Y.; McGuire, A. F.; Krason, M.; Molina-Lopez, F.; Ham, J.; Kraft, U.; Lee, Y.; Yun, Y.; Tok, J. B. H.; Bao, Z. An Integrated Self-Healable Electronic Skin System Fabricated *via* Dynamic Reconstruction of a Nanostructured Conducting Network. *Nat. Nanotechnol.* **2018**, *13* (11), 1057−1065.

(4) Roche, E. T.; Horvath, M. A.; Wamala, I.; Alazmani, A.; Song, S.-E.; Whyte, W.; Machaidze, Z.; Payne, C. J.; Weaver, J. C.; Fishbein, G.; Kuebler, J.; Vasilyev, N. V.; Mooney, D. J.; Pigula, F. A.; Walsh, C. J. Soft Robotic Sleeve Supports Heart Function. *Sci. Transl. Med.* **2017**, *9* (373), No. eaaf3925.

(5) Markvicka, E. J.; Bartlett, M. D.; Huang, X.; Majidi, C. An Autonomously Electrically Self-Healing Liquid Metal−Elastomer Composite for Robust Soft-Matter Robotics and Electronics. *Nat. Mater.* **2018**, *17* (7), 618−624.

(6) Ko, Y.; Kwon, M.; Bae, W. K.; Lee, B.; Lee, S. W.; Cho, J. Flexible Supercapacitor Electrodes Based on Real Metal-Like Cellulose Papers. *Nat. Commun.* **2017**, *8* (1), 536.

(7) Mackanic, D. G.; Chang, T.-H.; Huang, Z.; Cui, Y.; Bao, Z. Stretchable Electrochemical Energy Storage Devices. *Chem. Soc. Rev.* **2020**, *49* (13), 4466−4495.

(8) Ould Ely, T.; Kamzabek, D.; Chakraborty, D. Batteries Safety: Recent Progress and Current Challenges. *Front. Energy Res.* **2019**, *7*, 71.

(9) Choi, S.; Kwon, T.-w.; Coskun, A.; Choi, J. W. Highly Elastic Binders Integrating Polyrotaxanes for Silicon Microparticle Anodes in Lithium-Ion Batteries. *Science* **2017**, *357* (6348), 279−283.

(10) Zhou, Y.; Maleski, K.; Anasori, B.; Thostenson, J. O.; Pang, Y.; Feng, Y.; Zeng, K.; Parker, C. B.; Zauscher, S.; Gogotsi, Y.; Glass, J. T.; Cao, C. Ti_3C_2Tx MXene-Reduced Graphene Oxide Composite Electrodes for Stretchable Supercapacitors. *ACS Nano* **2020**, *14* (3), 3576−3586.

(11) Zhou, Y.; Parker, C. B.; Joshi, P.; Naskar, A. K.; Glass, J. T.; Cao, C. 4D Printing of Stretchable Supercapacitors *via* Hybrid Composite Materials. *Adv. Mater. Technol.* **2021**, *6* (1), 2001055.

(12) Pang, Y.; Cao, Y.; Chu, Y.; Liu, M.; Snyder, K.; MacKenzie, D.; Cao, C. Additive Manufacturing of Batteries. *Adv. Funct. Mater.* **2020**, *30* (1), 1906244.

(13) Etacheri, V.; Marom, R.; Elazari, R.; Salitra, G.; Aurbach, D. Challenges in The Development of Advanced Li-Ion Batteries: a Review. *Energy Environ. Sci.* **2011**, *4* (9), 3243−3262.

(14) Vlad, A.; Singh, N.; Galande, C.; Ajayan, P. M. Design Considerations for Unconventional Electrochemical Energy Storage Architectures. *Adv. Energy Mater.* **2015**, *5* (19), 1402115.

(15) Liu, W.; Chen, J.; Chen, Z.; Liu, K.; Zhou, G.; Sun, Y.; Song, M.-S.; Bao, Z.; Cui, Y. Stretchable Lithium-Ion Batteries Enabled by Device-Scaled Wavy Structure and Elastic-Sticky Separator. *Adv. Energy Mater.* **2017**, *7* (21), 1701076.

(16) Weng, W.; Sun, Q.; Zhang, Y.; He, S.; Wu, Q.; Deng, J.; Fang, X.; Guan, G.; Ren, J.; Peng, H. A Gum-Like Lithium-Ion Battery Based on a Novel Arched Structure. *Adv. Mater.* **2015**, *27* (8), 1363−1369.

(17) Liang, J.; Wang, S.; Yu, H.; Zhao, X.; Wang, H.; Tong, Y.; Tang, Q.; Liu, Y. Solution-Processed PDMS/SWCNT Porous Electrodes with High Mass Loading: Toward High Performance All-Stretchable-Component Lithium Ion Batteries. *Sustain. Energy Fuels* **2020**, *4*, 2718.

(18) Li, H.; Ding, Y.; Ha, H.; Shi, Y.; Peng, L.; Zhang, X.; Ellison, C. J.; Yu, G. An All-Stretchable-Component Sodium-Ion Full Battery. *Adv. Mater.* **2017**, *29* (23), 1700898.

(19) Xu, S.; Zhang, Y.; Cho, J.; Lee, J.; Huang, X.; Jia, L.; Fan, J. A.; Su, Y.; Su, J.; Zhang, H.; Cheng, H.; Lu, B.; Yu, C.; Chuang, C.; Kim, T.-i.; Song, T.; Shigeta, K.; Kang, S.; Dagdeviren, C.; Petrov, I.; et al. Stretchable Batteries with Self-Similar Serpentine Interconnects and Integrated Wireless Recharging Systems. *Nat. Commun.* **2013**, *4*, 1543.

(20) Gaikwad, A. M.; Zamarayeva, A. M.; Rousseau, J.; Chu, H.; Derin, I.; Steingart, D. A. Highly Stretchable Alkaline Batteries Based on an Embedded Conductive Fabric. *Adv. Mater.* **2012**, *24* (37), 5071−5076.

(21) Ren, J.; Zhang, Y.; Bai, W.; Chen, X.; Zhang, Z.; Fang, X.; Weng, W.; Wang, Y.; Peng, H. Elastic and Wearable Wire-Shaped Lithium-Ion Battery with High Electrochemical Performance. *Angew. Chem.* **2014**, *126* (30), 7998−8003.

(22) Xu, Y.; Zhao, Y.; Ren, J.; Zhang, Y.; Peng, H. An All-Solid-State Fiber-Shaped Aluminum−Air Battery with Flexibility, Stretchability, and High Electrochemical Performance. *Angew. Chem., Int. Ed.* **2016**, *55* (28), 7979−7982.

(23) Kumar, R.; Shin, J.; Yin, L.; You, J.-M.; Meng, Y. S.; Wang, J. All-Printed, Stretchable Zn-Ag_2O Rechargeable Battery *via* Hyperelastic Binder for Self-Powering Wearable Electronics. *Adv. Energy Mater.* **2017**, *7* (8), 1602096.

(24) Song, W.-J.; Park, J.; Kim, D. H.; Bae, S.; Kwak, M.-J.; Shin, M.; Kim, S.; Choi, S.; Jang, J.-H.; Shin, T. J.; Kim, S. Y.; Seo, K.; Park, S. Jabuticaba-Inspired Hybrid Carbon Filler/Polymer Electrode for Use in Highly Stretchable Aqueous Li-Ion Batteries. *Adv. Energy Mater.* **2018**, *8* (10), 1702478.

(25) Kettlgruber, G.; Kaltenbrunner, M.; Siket, C. M.; Moser, R.; Graz, I. M.; Schwödiauer, R.; Bauer, S. Intrinsically Stretchable and Rechargeable Batteries for Self-Powered Stretchable Electronics. *J. Mater. Chem. A* **2013**, *1* (18), 5505−5508.

(26) Gu, M.; Song, W.-J.; Hong, J.; Kim, S. Y.; Shin, T. J.; Kotov, N. A.; Park, S.; Kim, B.-S. Stretchable Batteries with Gradient Multilayer Conductors. *Sci. Adv.* **2019**, *5* (7), No. eaaw1879.

(27) Kang, S.; Hong, S. Y.; Kim, N.; Oh, J.; Park, M.; Chung, K. Y.; Lee, S.-S.; Lee, J.; Son, J. G. Stretchable Lithium-Ion Battery Based on Re-Entrant Micro-Honeycomb Electrodes and Cross-Linked Gel Electrolyte. *ACS Nano* **2020**, *14* (3), 3660−3668.

(28) Mackanic, D. G.; Yan, X.; Zhang, Q.; Matsuhisa, N.; Yu, Z.; Jiang, Y.; Manika, T.; Lopez, J.; Yan, H.; Liu, K.; Chen, X.; Cui, Y.; Bao, Z. Decoupling of Mechanical Properties and Ionic Conductivity in Supramolecular Lithium Ion Conductors. *Nat. Commun.* **2019**, *10* (1), 5384.

(29) Chen, X.; Huang, H.; Pan, L.; Liu, T.; Niederberger, M. Fully Integrated Design of a Stretchable Solid-State Lithium-Ion Full Battery. *Adv. Mater.* **2019**, *31*, 1904648.

(30) Ko, Y.; Oh, J.; Park, K. T.; Kim, S.; Huh, W.; Sung, B. J.; Lim, J. A.; Lee, S.-S.; Kim, H. Stretchable Conductive Adhesives with Superior Electrical Stability as Printable Interconnects in Washable Textile Electronics. *ACS Appl. Mater. Interfaces* **2019**, *11* (40), 37043−37050.

(31) van de Witte, P.; Dijkstra, P. J.; van den Berg, J. W. A.; Feijen, J. Phase Separation Processes in Polymer Solutions in Relation to Membrane Formation. *J. Membr. Sci.* **1996**, *117* (1), 1−31.
(32) Yang, H. M.; Kwon, Y. K.; Lee, S. B.; Kim, S.; Hong, K.; Lee, K. H. Physically Cross-Linked Homopolymer Ion Gels for High Performance Electrolyte-Gated Transistors. *ACS Appl. Mater. Interfaces* **2017**, *9* (10), 8813−8818.
(33) Sui, Y.; Wang, Z.; Gao, C. A New Synthetical Process of PVDF Derivatives *via* Atom Transfer Radical Graft Polymerizations and Its Application in Fabrication of Antifouling and Antibacterial PVDF Ultrafiltration Membranes. *Desalination Water Treat.* **2014**, *52* (34−36), 6377−6388.
(34) Gebrekrstos, A.; Prasanna Kar, G.; Madras, G.; Misra, A.; Bose, S. Does the Nature of Chemically Grafted Polymer onto PVDF Decide the Extent of Electroactive β-polymorph? *Polymer* **2019**, *181*, 121764.
(35) He, Y.; Miao, J.; Jiang, Z.; Tu, K.; Yang, H.; Chen, S.; Zhang, L.; Zhang, R. Improving the Anti-Fouling Property and Permeate Flux of Hollow Fiber Composite Nanofiltration Membrane Using β-cyclodextrin. *Sci. Rep.* **2019**, *9* (1), 12435.
(36) Cai, X.; Lei, T.; Sun, D.; Lin, L. A Critical Analysis of the α, β and γ Phases in Poly(vinylidene Fluoride) Using FTIR. *RSC Adv.* **2017**, *7* (25), 15382−15389.
(37) Martins, P.; Lopes, A. C.; Lanceros-Mendez, S. Electroactive Phases of Poly(vinylidene Fluoride): Determination, Processing and Applications. *Prog. Polym. Sci.* **2014**, *39* (4), 683−706.
(38) Lu, B.; Lamnawar, K.; Maazouz, A.; Sudre, G. Critical Role of Interfacial Diffusion and Diffuse Interphases Formed in Multi-Micro-/Nanolayered Polymer Films Based on Poly(vinylidene Fluoride) and Poly(methyl Methacrylate). *ACS Appl. Mater. Interfaces* **2018**, *10* (34), 29019−29037.
(39) Zamarayeva, A. M.; Ostfeld, A. E.; Wang, M.; Duey, J. K.; Deckman, I.; Lechêne, B. P.; Davies, G.; Steingart, D. A.; Arias, A. C. Flexible and Stretchable Power Sources for Wearable Electronics. *Sci. Adv.* **2017**, *3* (6), No. e1602051.

https://doi.org/10.1021/acsnano.1c08405
ACS Nano 2022, 16, 2271−2281